Nondilute diffusion from first principles: Li diffusion in Li_xTiS_2

Anton Van der Ven, John C. Thomas, and Qingchuan Xu
Department of Materials Science and Engineering, The University of Michigan, Ann Arbor, Michigan 48109, USA

Benjamin Swoboda and Dane Morgan
Department of Materials Science and Engineering, The University of Wisconsin Madison, Madison, Wisconsin 53706, USA
(Received 18 June 2008; revised manuscript received 27 August 2008; published 26 September 2008)

We investigate Li diffusion in the favorable intercalation compound Li_xTiS_2 as a function of Li concentration, x, from first principles. We find that Li ions hop between neighboring octahedral interstitial sites of the TiS_2 host by passing through an adjacent tetrahedral site. The migration barriers for these hops are significantly reduced when the end points belong to a divacancy. We use a cluster expansion within kinetic Monte Carlo simulations to describe the configuration dependence of the migration barriers and predict a diffusion coefficient that varies by several orders of magnitude with Li concentration, exhibiting a maximum close to $x=0.5$. The kinetic Monte Carlo simulations predict that diffusion is mediated predominantly by divacancies. We also find that the migration barriers depend strongly on the c-lattice parameter, which decreases as Li ions are removed from Li_xTiS_2.

DOI: 10.1103/PhysRevB.78.104306 PACS number(s): 66.30.Dn

I. INTRODUCTION

Intercalation compounds form a remarkable class of materials that are capable of reversibly absorbing large quantities of guest atoms at room temperature without undergoing major structural modification. While graphite is probably the most familiar intercalation compound, other examples include oxides [Li_xCoO_2, Na_xCoO_2, Li_xFePO_4, and $Ni(OH)_2$], sulfides (Li_xTiS_2, Ag_xTiS_2, and Li_xTaS_2), polymers, and organic molecular crystals.[1–4] A common feature among all intercalation compounds is their open and flexible crystal structure, which acts as host for intercalating guest ions or molecules.[5,6] Depending on the chemistry and structure of the host, guest species can range from alkali metals, to halides, to hydrogen, and even include molecules such as H_2O, OH^-, and CO_3^{2-}.[6,7] The electronic structure of the host is modified upon intercalation of a guest with the same intercalation compound often exhibiting a variety of electronic, magnetic, and optical properties as the concentration is changed. Na_xCoO_2, for example, possesses favorable thermoelectric properties[8] and becomes superconducting at low temperature upon removal of 66% Na and simultaneous intercalation of water molecules.[9]

Guest species can be intercalated electrochemically, enabling precise control over concentration. As a result, several intercalation compounds have proven to be superb electrodes in primary and secondary batteries.[1,3,4] The anode of a Li battery is often graphite, which intercalates Li between its two-dimensional graphitic sheets, while the cathode is typically a transition-metal oxide such as Li_xCoO_2 or Li_xFePO_4, in which Li occupies interstitial sites of the oxygen or phosphate framework.[1–5] The ability to electrochemically tune electronic, magnetic, and optical properties of intercalation compounds also makes these materials attractive for many other applications, including electrochromic displays.[10]

The kinetics of room-temperature intercalation processes plays a crucial role in determining the performance of a battery or an electrochromic device. Increasing the composition of guest ions within the intercalation compound, for example, requires diffusion of the guest species from the surface to the interior of the particle. Since the composition of the intercalating specie can vary from zero to complete filling of available interstitial sites of the host, diffusion predominantly occurs in nondilute regimes where short-range and long-range order among the intercalating species imposes complex correlations between successive atomic hops.[11]

The large variety of intercalation compound crystal structures and chemistries leads to qualitative differences of diffusion mechanisms that remain poorly understood and largely uncharacterized. Many important lithium intercalation compounds have a layered crystal structure in which Li intercalates between two-dimensional transition-metal oxide or transition-metal sulfide slabs.[1,5] The layered intercalation compounds exhibit several crystallographic variants differing in slab structure and in the manner in which the slabs are stacked.[5] The local crystallographic environment available to guest ions affects the type of long-range and short-range order that prevails among guest ions at nondilute concentrations as well as atomic hop mechanisms and barriers.

In an effort to contribute to our understanding of the role of stacking and anion chemistry on Li diffusion in layered intercalation compounds, we investigate diffusion in Li_xTiS_2 from first principles. While Li_xTiS_2 is no longer considered an attractive cathode material for Li-ion batteries due to its low voltage compared to that of transition-metal oxides such as Li_xCoO_2, Li_xNiO_2, and $Li_xCo_{0.33}Ni_{0.33}Mn_{0.33}O_2$, it was recognized early on as having favorable intercalation kinetics.[1,4] In part this can be attributed to the fact that Li removal from $LiTiS_2$ does not lead to structural modifications of the host as what occurs, for example, in Li_xCoO_2 below $x\sim0.3$.[12–15] Compared to the ionic bonding that characterizes transition-metal oxides, bonding within the sulfides tends to be more covalent;[16,17] however, it is not clear how these differences in bonding affect migration barriers for Li transport. Although the TiS_2 slabs have the same structure as the MO_2 slabs of many Li transition-metal oxides, the higher

degree of covalency in Li_xTiS_2 leads to a different stacking sequence of the slabs from that which typically prevails in the more ionic transition-metal oxides. Variations in stacking sequence should also lead to difference in Li-transport mechanisms.

The goal of this work is to elucidate collective transport in concentrated intercalation compounds from first principles. The approach uses atomic-scale energies from first principles to parametrize an easily evaluated cluster expansion Hamiltonian, which can then be used in thermodynamic [Monte Carlo (MC)] and kinetic (kinetic Monte Carlo) simulations to determine diffusion constants. In Sec. II, we describe a Kubo-Green formalism to calculate diffusion coefficients for interstitial diffusion in the nondilute regime with kinetic Monte Carlo simulations. These simulations require an accurate description of the dependence of the migration barriers for Li diffusion on local Li concentration and degree of order. To this end, we introduce a mixed-basis cluster expansion to describe the configuration dependence of migration barriers in nondilute solids. In Sec. III, we apply this formalism to predict the finite-temperature thermodynamic properties of Li_xTiS_2 as well as its concentration dependent Li diffusion coefficients. The results are discussed and compared with current understanding of diffusion mechanisms in lithium transition-metal oxides in Sec. IV.

II. METHOD

At the macroscopic level, Li transport within intercalation compounds can be described by Fick's first law, which relates the Li flux to a gradient in Li concentration through a proportionality constant called the Li chemical diffusion coefficient D. This chemical diffusion coefficient is a macroscopic metric for the Li-ion mobility within the host crystal structure and typically depends on the overall Li concentration. The chemical diffusion coefficient can be factored as a product of a self-diffusion coefficient, D_J, and a thermodynamic factor, Θ, according to[18]

$$D = D_J \Theta. \tag{1}$$

The thermodynamic factor, Θ, serves as a measure for the deviation of the Li chemical potential from thermodynamic ideality. It emerges when deriving Fick's first law from the more rigorous phenomenological flux expressions from irreversible thermodynamics that relate the Li flux, not to a gradient in concentration but to a gradient in chemical potential.[19] The thermodynamic factor for interstitial diffusion can be conveniently expressed as[18]

$$\Theta = \frac{\partial\left(\frac{\mu_{\mathrm{Li}}}{k_B T}\right)}{\partial \ln x}, \tag{2}$$

where μ_{Li} corresponds to the Li chemical potential, k_B to Boltzmann constant, T to the absolute temperature, and x to the Li concentration (the fraction of interstitial Li sites within the host occupied by Li).

The self-diffusion coefficient, D_J, contains all the kinetic information about the diffusing Li ions but is also indirectly affected by thermodynamic properties such as the equilibrium degree of short-range and long-range order, as this can influence ionic mobility. Within the linear response theory of the statistical mechanics of kinetic processes occurring close to equilibrium, we can relate kinetic rate coefficients such as D_J to fluctuations that occur at equilibrium. For interstitial diffusion, the self-diffusion coefficient can be written as[18,20–22]

$$D_J = \frac{1}{2dt}\frac{1}{N}\left\langle \left[\sum_{i=1}^{N} \Delta R_i(t)\right]^2 \right\rangle, \tag{3}$$

where t is the time, d is the dimension of the interstitial lattice ($d=2$ for two-dimensional diffusion as in $LiTiS_2$), N is the number of Li ions within the crystal, and $\Delta R_i(t)$ are vectors that connect the end points of the trajectory of the ith Li ion after time t. The brackets indicate an ensemble average. The self-diffusion coefficient is a metric of the square of the displacement of the center of mass of all diffusing Li ions after time t and therefore measures a collective mobility. If cross correlations between different diffusing Li ions are neglected when evaluating the square in Eq. (3), we obtain an expression for the tracer diffusion coefficient,[18]

$$D^* = \frac{1}{2dt}\frac{1}{N}\sum_{i=1}^{N} \langle [\Delta R_i(t)]^2 \rangle, \tag{4}$$

which measures the individual Li mobility.

The various metrics of Li mobility can be calculated numerically with kinetic Monte Carlo simulations,[23,24] which sample representative Li trajectories, provided an accurate description of individual stochastic hop events is available. The trajectories for each Li ion are a result of a sequence of individual atomic hops that occur with frequencies that can be approximated with transition state theory by[25]

$$\Gamma = \nu^* \exp\left(\frac{-\Delta E}{k_B T}\right), \tag{5}$$

where ΔE is the activation barrier. The vibrational prefactor ν^* within the harmonic approximation can be written as

$$\nu^* = \frac{\prod_{i}^{3M} \nu_i}{\prod_{j}^{3M-1} \nu_j'}. \tag{6}$$

The ν_i are the $3M$ normal-mode vibrational frequencies of the solid when the migrating atom resides at the initial state of the hop and the ν_j' are the $3M-1$ nonimaginary normal-mode vibrational frequencies of the solid when the migrating atom resides at the saddle point of the hop corresponding to the activated state (M is the total number of atoms in the solid). The activation barrier ΔE, as emerges in Vineyard's[25] derivation of Eq. (5), is equal to the difference in energy of the fully relaxed activated state and the fully relaxed initial state of the hop. Additional contributions to the activation free energy, e.g., from anharmonic contributions and changes

in electronic or magnetic states during the transition, are not included in the above expression.

In an intercalation compound, the thermodynamic factor and kinetic quantities such as ν_i, ν_i', and ΔE depend on the spatial and temporal variations of the degree of configurational disorder within the solid (Li-vacancy disorder in Li_xTiS_2). This dependence on the local configuration needs to be accounted for in kinetic Monte Carlo simulations. It is here that the cluster expansion formalism from alloy theory[11,26–28] becomes invaluable as a tool to extrapolate accurate first-principles migration barriers calculated for a few atomic arrangements to determine the migration barrier for any arrangement of atoms in a crystalline solid. The cluster expansion makes it possible to rapidly obtain accurate environment dependent on-lattice energies and hopping barriers necessary to determine transition rates. The speed of the cluster expansion energy calculations makes conventional and kinetic Monte Carlo simulations practical. With a cluster expansion, kinetic Monte Carlo is used to sample large numbers of trajectories of interacting diffusing particles to enable the evaluation of Kubo-Green expressions for the self-diffusion coefficients, Eq. (3),[11,28] while conventional Monte Carlo generates thermodynamic data to obtain the thermodynamic factor [Eq. (2)].[11] The results of the Monte Carlo simulations can then be combined to give the complete diffusion coefficient according to Eq. (1).

The cluster expansion formalism is a general tool to represent the configuration dependence of a physical property of a crystal such as the total energy.[26,27] Here we introduce a generalization of the usual approach by using two distinct basis sets, which we will call a mixed-basis cluster expansion. The mixed-basis approach is used here to take advantage of dilute occupancy on one sublattice to simplify the cluster expansion. We will consider a binary alloy (Li and vacancies) only. Generalization to multicomponent systems is formally straightforward (although often difficult in practice due to an explosion of terms in the expansion). The cluster expansion basis for a lattice is obtained by taking the tensor products of a set of basis functions for each lattice site. We can distinguish between two common basis-function sets to denote occupancy on a site: the *spin basis* and the *occupation basis*. The spin basis for a particular site i has the form $\{1,\sigma_i\}$, where $\sigma_i=1$ if site i has a Li and $\sigma_i=-1$ if the site is vacant, while the occupation basis has the form $\{1,p_j\}$, where $p_j=1$ if the site j has a Li and $p_j=0$ if the site is vacant. A particular arrangement within the crystal is then fully characterized by a vector of occupation variables $\{\vec{\sigma},\vec{p}\}=\{\sigma_1,\ldots,\sigma_{M_S},p_1,\ldots,p_{M_O}\}$, where M_S is the number of sites characterized with a spin basis and M_O is the number of sites characterized with an occupation basis.

Different basis choices have different advantages. The spin variables are useful for defining an orthonormal basis, which can aid in formal manipulation and may enhance the stability of fitting especially in nondilute regimes. However, the occupation basis has the advantage that the basis functions p_j are strictly zero for vacancies, which allows simplification for dilute Li concentrations through not writing terms that are zero (we will see this below). The occupation basis also has advantages when working with many species as discussed in Ref. 29.

Any property of a crystal that depends on configuration (e.g., fully relaxed total energy) can be expanded in terms of polynomials of the basis functions for each site. These polynomials, also referred to as cluster functions, consist of products of basis functions for sites belonging to different clusters of sites within the crystal. A general cluster expansion using two different basis sets can be written as

$$E(\vec{\sigma},\vec{p}) = \sum_{\alpha\in L_s} J_\alpha \phi_\alpha(\vec{\sigma}) + \sum_{\beta\in L_o} J_\beta \psi_\beta(\vec{p}) + \sum_{\alpha\in L_s,\beta\in L_o} J_{\alpha\beta}\phi_\alpha(\vec{\sigma})\psi_\beta(\vec{p}), \quad (7)$$

where L_s and L_o are the sublattices described with spin and occupation bases, respectively, and α and β are clusters of sites (e.g., point, pair, triplet, etc., clusters) on L_s and L_o, respectively. The ϕ_α are cluster functions and are equal to the product of spin basis functions on the sites of the cluster α. The ψ_β are analogous cluster functions for the occupation basis and are equal to products of the occupation basis cluster functions on the sites of β. Explicitly, the cluster functions can be written as

$$\phi_\alpha = \prod_{i\in\alpha}\sigma_i; \quad \psi_\beta = \prod_{j\in\beta} p_j.$$

The sum over α in Eq. (7) is taken to include the empty cluster but this is not included in the sum over β or the double sum over α and β to avoid double counting. The coefficients of the cluster functions in Eq. (7) are called effective cluster interactions (ECI).

Equation (7) is general for a binary system using the two basis sets on two different sublattices (e.g., octahedral sites and tetrahedral sites for Li occupancy in Li_xTiS_2). We now restrict the application to cases where the sublattice described with the occupation basis has dilute Li concentrations. This will be the case for the tetrahedral sites in the Li_xTiS_2 system. The use of the occupation basis allows a simple expression in the dilute limit if we assume that two Li on the occupation sublattice, L_o, never interact. Then the second term in Eq. (7) reduces to point contributions from the occupation lattice with all other terms automatically equal to zero since they contain a factor $p_i=0$. This simplification does not occur if the spin basis is used on the occupation lattice since no cluster function is zero for any occupation. We now use the simplification allowed by the dilute occupation of the occupation lattice to rewrite Eq. (7) as

$$E(\vec{\sigma},\vec{p}) = \sum_{\alpha\in L_s} J_\alpha\phi_\alpha(\vec{\sigma}) + \sum_{\alpha\in L_s, j\in L_o} J_{\alpha j}\phi_\alpha(\vec{\sigma})p_j. \quad (8)$$

We will use Eq. (8) to represent the energy of Li on the octahedral (L_s) and tetrahedral (L_o) sublattices in Li_xTiS_2. The result of Eq. (8) shows that this formalism is equivalent to the local cluster expansion introduced in Refs. 11, 30, and 31, where the $J_{\alpha j}$ have a local symmetry enforced by point j. The above derivation rigorously connects the local cluster expansion introduced to describe activated states[11] to a more general formulation, showing that the local cluster expansion is equivalent to the full mixed-basis cluster expansion in the dilute limit on the occupation sublattice.

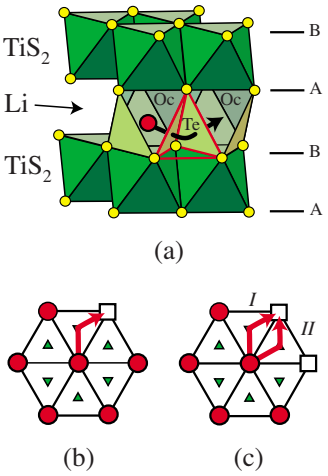

FIG. 1. (Color online) (a) Crystal structure of Li_xTiS_2 consisting of a periodic stacking of TiS_2 slabs between which Li ions can intercalate. The sulfur ions (circles) form a hexagonal close-packed sublattice, while the Ti and Li ions occupy alternating layers of octahedrally coordinated interstitial sites. Li migration between neighboring octahedral sites passes through adjacent tetrahedral sites [redrawn from (Ref. 43)]. (b) Li hop into an isolated vacancy (circles are Li, squares are vacancies, and triangles are tetrahedral sites within the Li layer). (c) Li hop into a divacancy.

III. RESULTS

The sulfur atoms of $LiTiS_2$ form two-dimensional triangular lattices stacked in an *ABAB* sequence[1,4] leading to a hexagonally close-packed anion sublattice. The Ti and Li ions alternately fill octahedral sites between the close-packed sulfur planes. The crystal can be viewed as an array of TiS_2 slabs separated by layers of Li [see Fig. 1(a)] and is often referred to as an O1 crystal structure using the nomenclature introduced by Delmas *et al.*[5] Due to the *ABAB* stacking sequence of the sulfur atoms, the Li ions occupy sites directly above and below the Ti ions. The Li-octahedral sites of the Li layer therefore share faces with the Ti-octahedral sites of the adjacent metal layers, a crystallographic feature that is absent in the more ionic oxide intercalation compounds having the O3 crystal structure, which are characterized by an *ABCABC* oxygen stacking sequence. This crystallographic difference between O1 $LiTiS_2$ and O3 layered transition-metal oxides leads to differences in Li transport characteristics between the two classes of materials.

A. Thermodynamics

The electrochemical removal of Li from $LiTiS_2$ results in the creation of Li vacancies between the TiS_2 slabs introducing configurational disorder. To describe the energy for arbitrary arrangements of the Li ions between the TiS_2 slabs, we constructed a binary cluster expansion expressed in terms of spin basis variables σ_i assigned to each octahedral site i that is +1 if a Li resides there and −1 if the site is vacant. Note that this corresponds to the spin basis portion of the cluster expansion described in Sec. II. The tetrahedral site properties will be described with the occupation basis, discussed in Sec. III C below. To parametrize the expansion coefficients of the

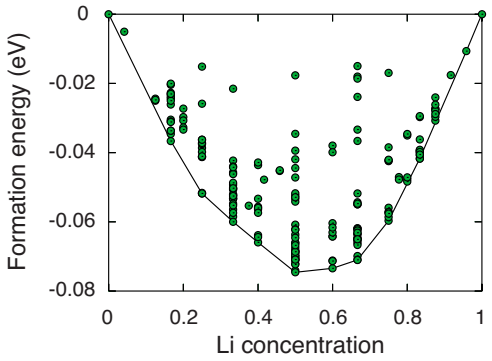

FIG. 2. (Color online) Calculated formation energies of 195 Li-vacancy configurations within the Li layers of Li_xTiS_2. The formation energies were calculated with LDA using the PAW method as implemented in VASP.

cluster expansion, we fit to the energies of 195 different Li-vacancy configurations over the octahedral sites of Li_xTiS_2, all calculated with local-density approximation (LDA) using projector augmented wave (PAW) pseudopotentials[32,33] as implemented in the VASP code.[34,35] We used LDA as this approximation to density-functional theory (DFT) correctly predicts the observed contraction of the c-lattice parameter of Li_xTiS_2 when the Li concentration is reduced below $x=0.5$,[36] while generalized gradient approximation (GGA) incorrectly predicts an expansion of the lattice parameter c with decreasing Li concentration. Past studies on layered transition-metal oxides demonstrated the sensitivity of migration barriers for Li diffusion to variations in the c-lattice parameter.[11,37] The equilibrium c-lattice parameters predicted by LDA for Li_xTiS_2 at various concentrations are consistently smaller than the experimental values. At $x=1$, for example, the predicted c-lattice parameter is 6.06 Å compared to an experimental value of approximately 6.2 Å (2.2%), while for $x=0$, the predicted c-lattice parameter is 5.48 Å compared to an experimental value of approximately 5.7 Å (3.9%).[36] All calculations were performed nonmagnetically as the inclusion of spin polarization had a negligible effect on the formation energies at different Li concentrations.

Figure 2 illustrates the calculated formation energies for the different configurations used in the fit of the cluster expansion where negative formation energies indicate a tendency for Li-vacancy ordering at intermediate Li concentrations. Below $x=0.25$, the most stable ordered phases correspond to staged configurations whereby Li ions segregate to alternating layers leaving the remaining layers empty. This is consistent with experimental observations of a nonuniform distribution of Li ions between alternating layers in Li_xTiS_2 at low Li concentrations.[36] In contrast to the staging transformations in Li_xC_6 graphite[38] and Li_xCoO_2,[13,14] the staging in Li_xTiS_2 is not accompanied by a shuffling of the TiS_2 slabs across the empty Li layers.

We used a least-squares fit to determine numerical values for the ECI of the cluster expansion and selected terms to be included in the expansion with a genetic algorithm that minimizes the cross-validation score of the fit.[39,40] The resulting cluster expansion contains 25 ECI corresponding to the empty cluster, point cluster, 11 pair clusters, nine triplet clus-

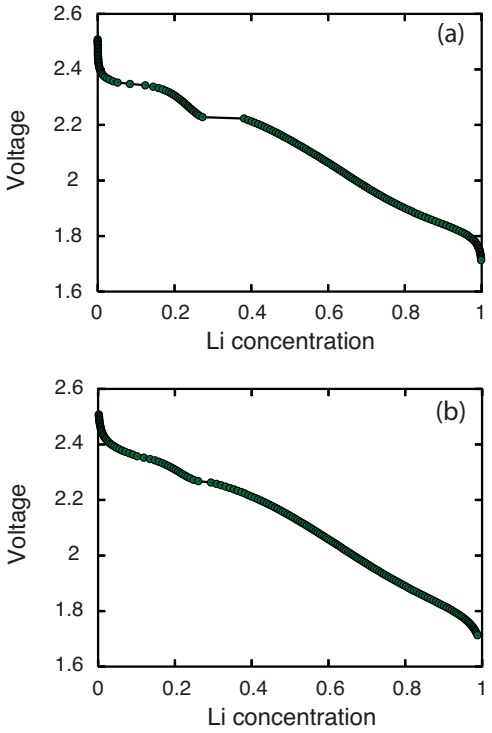

FIG. 3. (Color online) Calculated voltage curves at (a) 300 K and at (b) 450 K. The voltage curves were calculated with grand canonical Monte Carlo simulations applied to a cluster expansion for the configurational energy of Li-vacancy disorder over the octahedral sites of Li_xTiS_2.

ters, and three quadruplet clusters. The terms appearing in the cluster expansion include not only interactions between sites within the same Li layer but also between sites of adjacent Li layers. The root-mean-square error between the 195 LDA-PAW energies and the cluster-expanded values is 4 meV per Li_xTiS_2 formula unit, while the cross-validation score is 5 meV per Li_xTiS_2.

The cluster expansion can be implemented in grand canonical Monte Carlo simulations to calculate finite-temperature thermodynamic properties. Among them is the open cell voltage, which is linearly related to the Li chemical potential within Li_xTiS_2 according to the Nernst equation,

$$V(x) = -[\mu_{\mathrm{Li}}(x) - \mu_{\mathrm{Li}}^{\mathrm{reference}}]/e,$$

where $\mu_{\mathrm{Li}}(x)$ is the Li chemical potential in Li_xTiS_2 as a function of x (expressed in electron volt), $\mu_{\mathrm{Li}}^{\mathrm{reference}}$ is the Li chemical potential in the reference anode (which we take to be metallic Li and therefore constant), and e is the charge of an electron. Figure 3 illustrates calculated voltage curves for Li_xTiS_2 at 300 and 450 K. The sloping voltage profile indicates solid solution behavior characterized by an absence of any long-range order among Li ions and vacancies. The plateau between $x=0.28$ and 0.37 at 300 K corresponds to a first-order phase transformation between a stage I form of Li_xTiS_2 above $x=0.37$ (i.e., Li uniformly distributed between all Li layers) to a stage II form of Li_xTiS_2 below 0.28 (i.e., Li distributed between alternating Li layers only). Further Li removal leads to a second-order phase transformation from

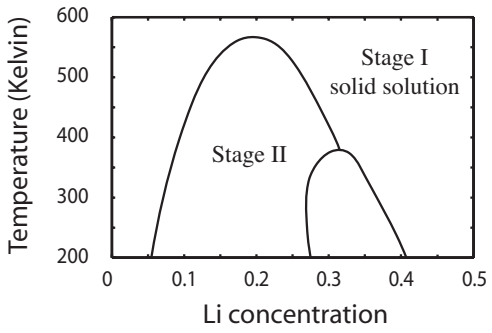

FIG. 4. Calculated temperature composition phase diagram of Li_xTiS_2.

the stage II compound to a dilute form of Li_xTiS_2 where Li ions are again uniformly distributed among all intercalation layers.

Monte Carlo simulations applied to the cluster expansion also allow us to construct a phase diagram depicting phase stability as a function of Li concentration and temperature. Figure 4 illustrates the calculated phase diagram for Li_xTiS_2 between 200 and 600 K. For most temperatures and compositions, Li_xTiS_2 exists as a solid solution with respect to Li ions and vacancies within the Li layers. Around $x=0.25$, however, the stage II form of Li_xTiS_2 is predicted to be stable in which the Li ions segregate to alternating Li layers. The stage II phase is stable upon heating up to 600 K and is separated from stage I solid solutions by a second-order transition line except at low temperature (below ~380 K) where a two-phase-coexistence region emerges. The two-phase-coexistence region was determined by comparing grand canonical free energies of the stage II and stage I phases obtained with free-energy integration of the chemical potential with respect to the average number of Li. The second-order transition lines were determined by tracking the temperature and compositions where an order parameter that characterizes the stage II phase becomes zero. Numerical inaccuracies during free-energy integration prevented a precise determination of the two-phase-coexistence bounds around 380 K where transition from stage II to stage I changes from first order to second order.

An important part of the chemical diffusion coefficient, D, according to Eq. (1), is the thermodynamic factor Θ. While the thermodynamic factor, given by Eq. (2), can be calculated by taking a numerical derivative of the Li chemical potential with respect to $\ln(x)$, it can also be determined directly in grand canonical Monte Carlo simulations by averaging over fluctuations in the number of Li ions at fixed chemical potential using[18]

$$\Theta = \frac{\langle N \rangle}{\langle (\langle N \rangle - N)^2 \rangle}, \tag{9}$$

where N is the number of Li ions in a Monte Carlo cell and the brackets correspond to ensemble averages at constant temperature and Li chemical potential. Figure 5 illustrates the calculated thermodynamic factor at 300 K as a function of the Li concentration. The gap between 0.28 and 0.37 is the two-phase region where the thermodynamic factor is not de-

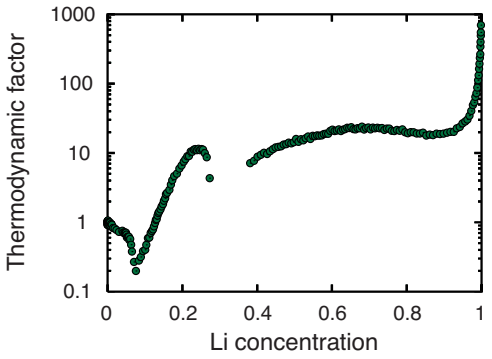

FIG. 5. (Color online) Calculated thermodynamic factor as a function of Li composition in Li_xTiS_2 at 300 K.

fined (similar gaps appear in Figs. 8–10). The thermodynamic factor can be viewed as a measure of the extent to which the compound deviates from thermodynamic ideality. In the dilute limit where interactions among Li ions are negligible, the thermodynamic factor is close to 1. As the Li ions begin to interact with each other with increasing concentration, the thermodynamic factor deviates from 1. The dip in the thermodynamic factor at $x \sim 0.07$ is a result of the second-order phase transformation at which fluctuations in Li density become very large. As the concentration corresponding to the second-order transition is approached, it becomes increasingly difficult to achieve a net Li flux by imposing a gradient in concentration. This is known as critical slowing down and is manifested in a decreasing thermodynamic factor.

The thermodynamic factor is larger than 1 at nondilute Li concentrations and away from the second-order phase transition. In Li_xTiS_2, Θ ranges between 10 and 20 for most Li concentrations diverging only as x approaches 1 where the deviation from thermodynamic ideality is the largest as then Li_xTiS_2 effectively becomes a stoichiometric compound that is very resistant to fluctuations in number of Li ions at fixed Li chemical potential [i.e., small denominator in Eq. (9)]. In fact, the thermodynamic factor always peaks at stoichiometric compositions where Li-vacancy ordering is thermodynamically stable,[11,41] although in Li_xTiS_2 ordering at stoichiometric compositions is absent above 300 K.

B. Hop mechanisms and migration barriers

Li diffusion in intercalation compounds occurs by a vacancy mechanism, whereby individual Li ions hop into neighboring vacant sites. Crystallographically, the least constricted pathway for Li migration between neighboring octahedral sites of layered transition-metal oxides and sulfides having the O3 and O1 crystal structure is through an adjacent tetrahedral site. This is schematically illustrated in Fig. 1(a). The Li-octahedral sites form a two-dimensional triangular lattice with the tetrahedral sites occupying approximately the center of each triangle [Fig. 1(b)]. Consistent with the crystallography of these compounds, first-principles investigations of diffusion in Li_xCoO_2 showed that favorable Li migration paths pass through tetrahedral sites,[11,42] while recent NMR measurements[43] have provided strong evidence that the same occurs in Li_xTiS_2. There are differences relevant for diffusion; however, between the O3 layered transition-metal oxides having an *ABCABC* oxygen stacking sequence and O1 $LiTiS_2$ with its *ABAB* sulfur stacking sequence. In the layered transition-metal oxides, the tetrahedral sites of the Li layers share faces with octahedral transition-metal sites, while in $LiTiS_2$ they do not. This leads to important differences in the energy landscape along a hop between the two classes of intercalation compounds.

The migration barriers in the layered intercalation compounds are very sensitive to the Li concentration and arrangement in the vicinity of the hopping Li ion.[11] A distinction can be made between two different local environments depending on the occupancy of neighboring octahedral sites surrounding the tetrahedral site along the hop path [Figs. 1(b) and 1(c)]. In one local environment, the tetrahedral site, when occupied by the migrating Li ion, has a neighboring Li in an adjacent octahedral site [Fig. 1(b)]. This local environment will occur when a Li ion migrates to an isolated vacancy surrounded by Li. A qualitatively different local environment exists when the migrating Li ion follows a path through a tetrahedral site that does not share a face with occupied octahedral sites. This local environment occurs when the end point of the hop belongs to a divacancy [Fig. 1(c)].

We explored the energy landscape along migration paths between neighboring octahedral Li sites in Li_xTiS_2 with the nudged-elastic band method as implemented in VASP. We used supercells containing 24 Li_xTiS_2 units ($2\sqrt{3}a \times 2\sqrt{3}a \times 2c$ supercell, where a and c are the primitive unit-cell lattice parameters) and performed calculations with a $3 \times 3 \times 3$ k-point grid. All nudged-elastic band calculations were performed at constant volume (using the fully relaxed volume and cell dimensions of the initial state of the hop). The images for the nudged-elastic band calculations were interpolated between Li occupancy in the initial octahedral site and Li occupancy of the intermediate tetrahedral site. In all configurations considered, the tetrahedral sites were found to be a low-energy stable intermediate state of a Li hop between neighboring octahedral sites.

Figure 6(a) illustrates the energy as a Li ion migrates into an isolated vacancy [Fig. 1(b)] calculated in a supercell containing 24 TiS_2 units and 23 Li ions. For this hop, each of the two tetrahedral sites, through which the Li ion can pass, shares a face with an occupied octahedral site. The difference in energy between the octahedral and tetrahedral sites is approximately 700 meV. The tetrahedral site is a shallow local minimum with a barrier to escape the tetrahedral site of less than 15 meV.

In contrast to a hop into an isolated vacancy, a Li ion migrating into a divacancy can follow two nonequivalent paths, each passing through a differently coordinated tetrahedral site [Fig. 1(c)]. Along one path [path I in Fig. 1(c)], the migrating Li ion in the tetrahedral site shares a face with an occupied octahedral site, while along the other path [path II in Fig. 1(c)] it does not. Figure 6(b) illustrates the energy along both paths showing a difference between the two tetrahedral sites of approximately 380 meV. Furthermore, there is a qualitative difference in the shape of the energy landscape along the two paths. Along path I the Li ion locally

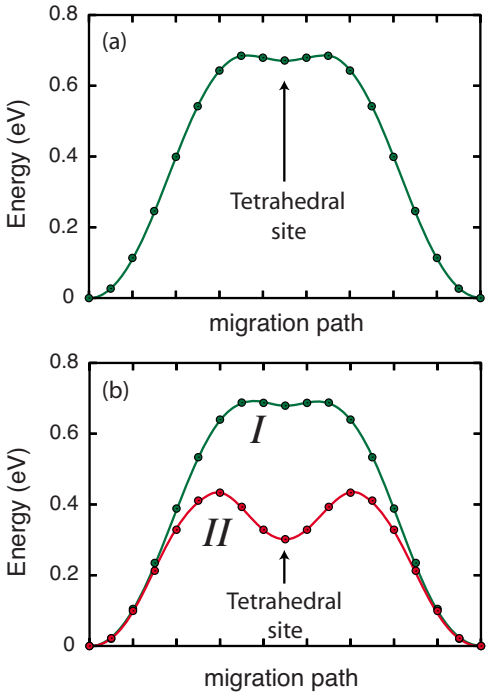

FIG. 6. (Color online) (a) Energy along minimal energy migration path for a Li hop into an isolated vacancy [see Fig. 1(b)] as calculated with the nudged-elastic band method using VASP. (b) Energy along paths I and II of Fig. 1(c) for a Li hop into a divacancy.

samples an identical environment as a Li ion migrating into an isolated vacancy [Fig. 1(b)]. The energy along this path is also very similar to that of a hop into an isolated vacancy [compare Figs. 6(a) with 6(b)]. The absence of occupied adjacent octahedral sites along path II renders the tetrahedral site energetically more favorable. Furthermore, the tetrahedral site along path II is a deep local minimum with an energy barrier of 150 meV to escape the tetrahedral site. The increased energy along path I as compared to that along path II is a result of the electrostatic repulsion when a Li ion enters a tetrahedral site that shares a face with an occupied octahedral site.

As the Li concentration is reduced, the number of vacancies and therefore also divacancies increases in Li_xTiS_2. Hence the importance of non-face-sharing tetrahedral sites as intermediate states of Li hops increases with decreasing Li concentration. Figure 7 illustrates energies along Li migration paths into a divacancy at various Li concentrations ranging from the dilute limit of one Li in a supercell of 24 Li sites to the concentrated limit of a Li ion migrating into an isolated divacancy. As is clear from Fig. 7, the energy profile as well as the relative height between the octahedral and intermediate tetrahedral sites depends strongly on Li concentration. A similar variation was predicted for Li_xCoO_2 and was shown to result from the strong dependence of the c-lattice parameter with decreasing Li concentration,[11] which disproportionately penalizes the tetrahedral site over the octahedral site.[37] As in $LiCoO_2$, the c-lattice parameter of Li_xTiS_2 also contracts with decreasing Li concentration below $x=0.5$, and this contraction is predicted with LDA. An important feature of the energy landscapes of Fig. 7 is that

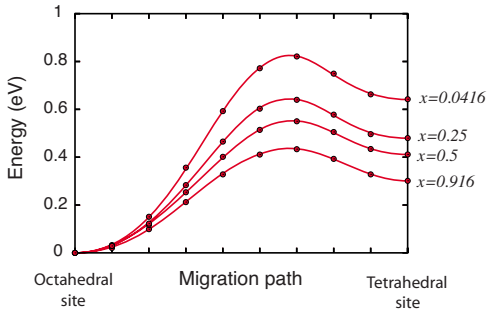

FIG. 7. (Color online) Energy along the migration path into a tetrahedral site belonging to a divacancy at four different Li concentrations. The increase in energy of the tetrahedral site with decreasing Li is primarily due to a contraction of the c-lattice parameter as Li is removed from Li_xTiS_2.

the tetrahedral sites while high in energy compared to the octahedral sites nevertheless correspond to relatively deep local minima. The barrier to escape a tetrahedral site is approximately 150 meV and varies negligibly with Li concentration (differing at most by 20 meV from the average 150 meV, which is within the numerical error of the supercell calculations). This implies that a migrating Li ion is likely to thermalize once it reaches the tetrahedral site resulting in a 1/3 probability that it returns to its original octahedral site and a 2/3 probability that it continues on to a different octahedral site (each tetrahedral site has three neighboring octahedral sites).

C. Kinetic Monte Carlo and diffusion

Interactions among Li ions of Li_xTiS_2 can significantly complicate a description of the collective transport behavior at nondilute Li concentrations. In the absence of long-range order, migrating Li ions in Li_xTiS_2 sample many different local environments along their trajectories with variations in the local configuration affecting the migration barriers ΔE. When sampling representative Li trajectories in kinetic Monte Carlo simulations to numerically evaluate expressions for diffusion coefficients, Eqs. (3) and (4), it is essential that the environment dependence of the migration barriers is accurately accounted for. In the previous section, we showed that a distinction can be made between two qualitatively different local environments. In one, the tetrahedral site along the migration path shares a face with an occupied octahedral site, while in the other the tetrahedral site does not share any faces with occupied octahedral sites. In the first environment, the tetrahedral site is a very shallow minimum with a barrier of $\sim$15 meV to escape the tetrahedral site. In the second environment the tetrahedral site corresponds to a deeper local minimum with a well depth of approximately 150 meV. Furthermore, while the well depth of 150 meV seems relatively insensitive to the overall Li concentration and local ordering (based on several nudged-elastic band calculations), the difference in energy between the tetrahedral sites and end-point octahedral sites does vary substantially with composition and local ordering.

To account for the configuration dependence of tetrahedral site occupancy, we follow the approach given in Sec. II

and introduce extra terms to our cluster expansion of Sec. III A to link the tetrahedral and octahedral sites. We use a mixed-basis cluster expansion, introducing an occupation variable p_j for each tetrahedral site j that is one if it is occupied by Li and zero if it is vacant. As discussed in Sec. II, the use of these occupation variables, as opposed to the spin basis (that can be 1 and −1), is more convenient in dilute concentration limits. Since the tetrahedral sites have significantly higher energies than the octahedral sites, they are rarely occupied and only as intermediate states of Li hops between neighboring octahedral sites. We parametrized the interaction coefficients that connect tetrahedral sites with octahedral sites by fitting to the energies of 27 configurations with one occupied tetrahedral site calculated in supercells containing 24 Li_xTiS_2 units. The root-mean-square error between the LDA-PAW formation energies for these configurations and the cluster expansion predicted formation energies is less than 3 meV per unit cell, and the leave one out cross-validation score is 4 meV per unit cell. The extra terms connecting the tetrahedral sites with octahedral sites included a point term (for the tetrahedral site), three pairs consisting of a tetrahedral site and a neighboring octahedral site, and two triplet terms connecting a tetrahedral site with two octahedral sites.

With the additional terms accounting for tetrahedral occupancy, we have an accurate cluster expansion that describes the configuration dependence of the end-point energies and the intermediate tetrahedral sites for any Li hop in Li_xTiS_2. Within our kinetic Monte Carlo simulations, we used Eq. (5) from transition state theory to calculate Li-ion hop frequencies. We used the following rules to determine the migration barrier for each hop. If the tetrahedral site along the migration path does not share faces with occupied octahedral sites, the barrier to migrate into the tetrahedral site is the difference in energy between the tetrahedral site and the initial octahedral site plus 150 meV. The barrier to escape the tetrahedral site is 150 meV. If the tetrahedral site along the migration path does share a face with an occupied octahedral site, then the barrier is the difference in energy between the tetrahedral and octahedral sites plus 15 meV. The barrier to escape those tetrahedral sites is 15 meV. For all hops, the energies of the tetrahedral and octahedral sites were calculated with the cluster expansion such that the effects of composition and local order/disorder on migration barriers are rigorously included. It should be noted that the treatment of the tetrahedral site as a stable local minimum in which the Li thermalizes is questionable for hops into tetrahedral sites that share a face with an occupied octahedral site since the well depth is only about 15 meV. However, as emerges from the kinetic Monte Carlo simulations, the generally high barrier of these types of hops makes them very rare events so their contribution to the overall diffusivity (except for high Li content) is negligible.

While we did not attempt to describe the dependence of the vibrational prefactors appearing in Eq. (5) on local configurational disorder, we used different values depending on whether the Li ion migrates into a tetrahedral site or out of a tetrahedral site. These values were calculated from first principles within the local harmonic approximation using VASP where gamma-point vibrational frequencies of the migrating Li-ion were determined by perturbing the atom performing

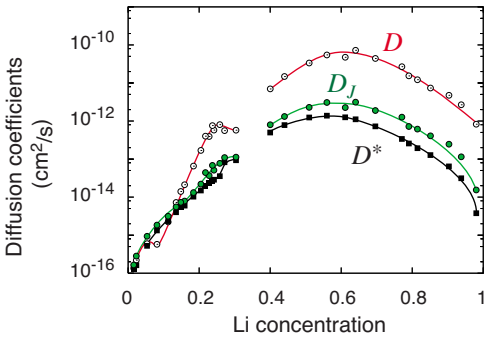

FIG. 8. (Color online) The tracer (black squares), self (filled circles), and chemical (empty circles) diffusion coefficients calculated with kinetic Monte Carlo simulations.

the hop and calculating restoring forces. Based on calculations in various configurations, we used a value of $\nu^*=5\times10^{12}$ Hz for Li hopping into a tetrahedral site if it does not share a face with an occupied octahedral site, $\nu^*=9.5\times10^{12}$ Hz for Li hopping out of this site, $\nu^*=3.5\times10^{12}$ Hz for Li hopping into a tetrahedral site if it shares a face with an occupied octahedral site, and $\nu^*=6.5\times10^{12}$ Hz for Li hops out of that site. These values are consistent with recent ^{7}Li spin alignment echo NMR measurements on Li_xTiS_2.[43]

To calculate diffusion coefficients at finite temperature, we used a standard kinetic Monte Carlo algorithm as first proposed by Bortz *et al.*[23] and described elsewhere.[11,24] The kinetic Monte Carlo simulation cell contained $12\times12\times12$ Li sites. For each Li concentration (initialized to be a random configuration), we performed 1000 Monte Carlo (MC) passes, where each MC pass corresponds to performing as many Li hops as there are Li sites. After each hop, the trajectories, $\Delta R_i(t)$, and the time were updated as described in, for example, Ref. 24. Values for the tracer and self-diffusion coefficients were collected for averaging purposes starting after the first 500 MC passes. The whole process was repeated 50 times starting from the Li configuration of the previous ensemble run, to ensure that sufficient uncorrelated values for D^* and D_J were sampled. For kinetic Monte Carlo simulations at concentrations where the stage II phase is predicted to be stable, we initiated the Monte Carlo cell by performing grand canonical Monte Carlo simulations and kept the last configuration after 1000 Monte Carlo passes. This ensured that the cell had a distribution of Li between alternating Li layers representative of the staged phase.

Figure 8 illustrates calculated diffusion coefficients at 300 K as a function of Li concentration. The chemical diffusion coefficient was obtained by multiplying the self-diffusion coefficient D_J with the thermodynamic factor Θ according to Eq. (1). As is clear from Fig. 8, the diffusion coefficients all have a very strong dependence on Li concentration exhibiting a maximum close to $x=0.5$ and varying by several orders of magnitude over the whole concentration interval. The diffusion coefficients decreases rapidly as the Li concentration is reduced below $x=0.55$. The tracer diffusion coefficient is also always less than the self-diffusion coefficient.

The kinetic Monte Carlo simulations show that Li transport is dominated by hops into divacancies. Figure 9 illus-

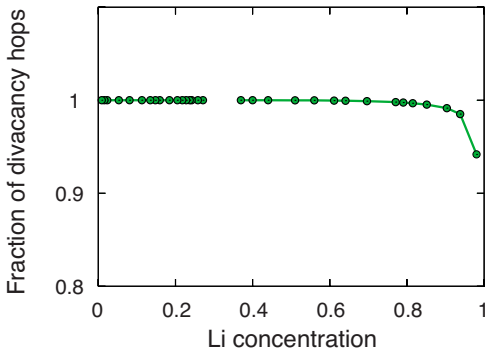

FIG. 9. (Color online) Fraction of Li hops into divacancies as a function of Li concentration. Only at concentrations close to $x=1$ is there any appreciable hopping into isolated Li vacancies.

trates the fraction of hops involving tetrahedral sites that do not share faces with occupied octahedral sites. These hops can only occur when the end point of the hop belongs to a divacancy. As is clear from Fig. 9, divacancy hops dominate over the entire concentration range with hops into isolated vacancies only occurring appreciably as x approaches one. The migration barriers associated with divacancies are significantly lower than those into isolated vacancies (which involve tetrahedral sites that share a face with an occupied octahedral site). However, the divacancy concentration is very low at high Li concentration, increasing with decreasing Li concentration. This is shown in Fig. 10, which illustrates the average number of divacancies around a Li ion as a function of concentration. The rapid increase in divacancy concentration as x is reduced from one is responsible for a similar increase in the diffusion coefficients. Below $x=0.55$, however, the diffusion coefficients decrease again in spite of the continued increase in the number of divacancies. This decrease in the diffusion coefficients results from an increase in the migration barriers at low Li concentration. As is clear from Fig. 7, the difference in energy between tetrahedral and octahedral occupancy increases with decreasing Li concentration due to a contraction of the c-lattice parameter. Within the kinetic Monte Carlo simulations, we are accurately capturing this concentration dependence of the energy difference between tetrahedral and octahedral occupancy with the cluster expansion.

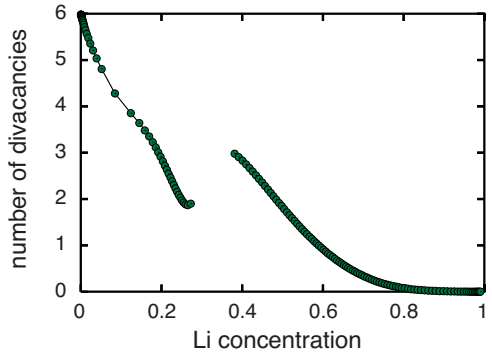

FIG. 10. (Color online) Equilibrium number of divacancies surrounding each Li ion as a function of Li concentration calculated with grand canonical Monte Carlo simulations.

IV. DISCUSSION

Common among the various layered transition-metal oxides and sulfides such as Li_xCoO_2, Li_xNiO_2, and Li_xTiS_2 is that Li hops between neighboring octahedral sites pass through (or close to) an intermediate tetrahedral site. Furthermore, Li migration barriers in all these intercalation compounds are substantially lower when the end point of the hop belongs to a divacancy as opposed to an isolated vacancy. The latter configuration results in a large electrostatic penalty as the migrating Li occupying the intermediate tetrahedral site then shares a face with an occupied octahedral site. As is demonstrated here for Li_xTiS_2 and in a previous study of Li diffusion in Li_xCoO_2 (Ref. 11) the dominant diffusion-mediating complex in the layered intercalation compounds is a divacancy. This leads to a strong concentration dependence of the diffusion coefficient at high Li concentration where the concentration of divacancies diminishes with Li concentration above $x=0.5$. Another commonality between the layered transition-metal oxides and Li_xTiS_2 is a tendency for the c-lattice parameter to contract significantly as Li is removed below $x=0.55$. This contraction penalizes the tetrahedral site over the octahedral site leading to higher migration barriers. The increase in migration barriers with decreasing Li concentration causes a drop in the diffusion coefficient at dilute Li concentrations.

The difference in stacking sequence between Li_xTiS_2 and the layered transition-metal oxides such as Li_xCoO_2 do result in qualitative differences in transport behavior between the two classes of materials. In the layered transition-metal oxides with *ABCABC* oxygen stacking, the tetrahedral sites in the Li layers are energetically penalized as they share a face with a transition-metal ion. In fact, a first-principles investigation of diffusion in Li_xCoO_2 showed that the tetrahedral site along a path connecting neighboring octahedral sites actually corresponds to an activated state (i.e., saddle point) at dilute lithium concentrations where the face-sharing Co ions have an effective valence close to +4.[11] At high Li concentrations where the effective valence of face-sharing Co ions is closer to +3, the tetrahedral site corresponds to a very shallow energy minimum with an energy barrier to leave the tetrahedral site of approximately 25 meV.[11]

In contrast to the oxides, the tetrahedral sites of Li_xTiS_2 do not share faces with the Ti ions. When the tetrahedral site is part of a divacancy, it corresponds to a relatively stable local minimum with well depth around 150 meV. The Li hops between neighboring octahedral sites should then occur in two steps with the migrating Li thermalizing in the tetrahedral site before performing a second hop to an octahedral site. This is consistent with claims made in a report on NMR measurements of Li diffusion in Li_xTiS_2.[43,44] The likelihood that Li ions will thermalize in the tetrahedral site before continuing with its trajectory reduces overall Li mobility in the layered crystal structure as these thermalized Li ions have a 1/3 probability to migrate back to its original octahedral site. Hence, when compared to hopping in Li_xCoO_2, although the tetrahedral sites in Li_xTiS_2 are not electrostatically penalized due to face-sharing transition-metal ions, their enhanced local stability reduces the efficiency of Li hops between neighboring octahedral sites.

To estimate the effect of intermediate thermalization in the tetrahedral sites on the tracer diffusion coefficient, we performed two types of kinetic Monte Carlo simulations in the dilute limit of a single Li ion: one set of simulations treated the tetrahedral sites as a metastable intermediate state (i.e., Li ions are assumed to thermalize in the tetrahedral site before continuing on), while the other set of simulations treated the tetrahedral sites as activated states. The hop frequencies when treating the tetrahedral sites as activated states were set equal to one-half the hop frequency needed to hop into the tetrahedral sites when assuming the tetrahedral sites as metastable states (the factor of 1/2 emerges because a Li hop through an activated tetrahedral site has two octahedral sites to choose from). In the limit of a single diffusing Li ion, every hop has the same migration barrier, thereby allowing us to isolate the effect of an intermediate metastable tetrahedral state from variations in migration barriers due to configurational disorder. For an isolated Li ion, the cluster expansion predicts a tetrahedral versus octahedral energy of 670 meV, which gives a barrier for the octahedral to tetrahedral site hop of 820 meV. Calculations of tracer diffusion coefficients (after averaging over 5000 independent runs) showed that thermalization in the tetrahedral sites (in the dilute limit) leads to a reduction in the tracer diffusion coefficient by a factor of approximately two-thirds compared to not allowing thermalization in the tetrahedral sites (this is consistent with the fact that when a Li ion thermalizes in a tetrahedral site it has a 1/3 chance to hop back to its initial state). At room temperature (300 K), the reduction factor of about 2/3 was found to be independent of whether the energy barrier to get out of the metastable tetrahedral site is 150 or 0 meV, which is consistent with the hop from the octahedral to tetrahedral sites being rate limiting (as is confirmed below).

A barrier of 150 meV to escape a tetrahedral site also does not have a measurable effect on the effective migration barrier as extracted from the slope of the natural logarithm of the tracer diffusion coefficient, D^*, versus $1/k_BT$, where D^* was calculated at temperature increments of 10 K between 250 and 350 K in the dilute limit of a single diffusing Li ion. In this temperature interval, the effective migration barrier extracted from the temperature dependence of D^* was equal (within the error of the least square regression) to the actual migration barrier within the kinetic Monte Carlo simulations to migrate into the tetrahedral site (both were about 820 meV). This implies that the rate-limiting steps for diffusion are hops from octahedral sites to tetrahedral sites.

Li diffusion coefficients and transport properties in Li_xTiS_2 have been investigated experimentally with various probes.[43–50] A common method of measuring Li diffusion coefficients in electrode materials is within an electrochemical cell. These measurements, however, introduce a variety of uncertainties related to the difficulty of precisely characterizing geometrical dimensions of the intercalation compound particles[47,49] as well as the difficulty to distinguish between Li diffusion in the intercalation compound from other dynamic processes occurring in the electrolyte, the counter electrode and at interfaces. NMR measurements have also been applied to elucidate Li transport mechanisms in Li_xTiS_2,[43–45,48,50] which is very powerful in probing atomic hop characteristics but provides less insight about correlated atomic transport at nondilute Li concentrations.

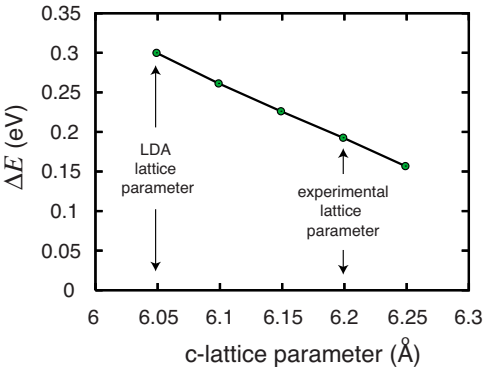

FIG. 11. (Color online) Variation of the energy of tetrahedral occupancy relative to octahedral occupancy next to a divacancy as a function of *c*-lattice parameter [ΔE is the difference in energy between the tetrahedral and octahedral sites of Fig. 1(c)].

Kanehori *et al.*[49] compared their electrochemically measured diffusion coefficients of single-crystal Li_xTiS_2 using current pulse and galvanostatic methods with previous measurements of Li diffusion coefficients in Li_xTiS_2 (Fig. 5 of Ref. 49). With the exception of one study reviewed by Kanehori *et al.*,[49] all measured diffusion coefficients have values between 10^{-9} and 10^{-7} cm^2/s depending on the Li concentration. The exception was a study by West *et al.*, which according to Kanehori *et al.*,[49] reported diffusion coefficients ranging between 10^{-11} and 2×10^{-10} cm^2/s. The qualitative dependence of Li diffusion coefficients on Li concentration in three of the studies are very similar to that predicted in this work, exhibiting low diffusion coefficients in the dilute (x close to zero) and concentrated (x close to one) regimes with large diffusion coefficients at intermediate concentrations. The measurements of Kanehori *et al.*,[49] for example, exhibit a maximum in the diffusion coefficient at $x=0.5$. A variety of these studies are complicated by the fact that the Li_xTiS_2 samples used in the measurements had excess Ti in the Li layer, which affects Li mobility by blocking sites and by modifying the equilibrium *c*-lattice parameter of the host.

While the qualitative variation of D with Li concentration predicted in this work is observed experimentally, there is a large quantitative discrepancy between measured and calculated diffusion coefficients. A major source of this discrepancy can be attributed to the under prediction of the *c*-lattice parameter with LDA as the calculated migration barriers are very sensitive to the *c*-lattice parameter. Figure 11 illustrates the variation of the difference in energy between tetrahedral and octahedral occupancies as a function of *c*-lattice parameter. These energies were calculated in a supercell containing 24 Li_xTiS_2 units with a Li divacancy. A variation of the *c*-lattice parameter by 3% leads to a change in the tetrahedral-octahedral energy difference by 150 meV. At room temperature, errors in migration barriers of this order will translate into an error in diffusion coefficients of two orders of magnitude due to the exponential dependence of the hop frequencies on migration barriers. LDA under predicts the *c*-lattice parameter in Li_xTiS_2 by values ranging between 2%–3.8% with a larger error in the *c*-lattice parameter at dilute Li concentrations. The increased error in *c* at

low x is likely the origin for a more dramatic drop in the calculated diffusion coefficients with decreasing Li concentration as compared to the experimentally measured coefficients at low Li concentrations. In general, predicted diffusion coefficients at low temperature will be very sensitive to DFT errors in calculated migration barriers, which, as in Li_xTiS_2, may originate in large part from the incorrect prediction of lattice parameters.

V. CONCLUSION

We have performed a first-principles investigation of Li diffusion in Li_xTiS_2 using a mixed-basis cluster expansion approach to describe the configuration dependence of the Li migration barriers in kinetic Monte Carlo simulations. First-principles electronic structure calculations within the local-density approximation to density-functional theory predict that Li migrates between neighboring octahedral sites by passing through an adjacent tetrahedral site. The migration barriers for Li hops are found to be very sensitive to the local environment with lower migration barriers occurring when Li hops into a divacancy as opposed to an isolated Li-vacancy. Furthermore, consistent with other layered intercalation compounds, we find that the migration barriers are very sensitive to the c-lattice parameter of the Li_xTiS_2 host structure. This leads to an increase in the migration barrier with decreasing Li concentration due to the contraction of the c-lattice parameter as Li is removed from Li_xTiS_2. The tracer, self, and chemical diffusion coefficients calculated by evaluating Kubo-Green expressions within kinetic Monte Carlo simulations all exhibit a maximum close to $x=0.5$ in qualitative agreement with experiment. The decrease in the diffusion coefficients at low Li concentration results from a contraction of the c-lattice parameter, while the decrease in diffusion coefficients at high Li concentration arises from a decrease in the concentration of diffusion-mediating divacancies. We attribute a large part of the quantitative disparity between calculated and measured diffusion coefficients to the systematic under prediction of the c-lattice parameter of Li_xTiS_2 with LDA, which is largest at dilute Li concentrations.

ACKNOWLEDGMENTS

We are grateful to Brian Puchala for helpful discussions. This research was supported in part by a grant from the petroleum research fund (PRF) of the American Chemical Society (ACS PRF Grant No. 46584-G10). D.M. and B.S. gratefully acknowledge support from the Department of Energy (DOE) Nuclear Engineering Research Initiative (NERI) Program under Award No. DE-FC07-06ID14747.

[1] M. S. Whittingham, Prog. Solid State Chem. **12**, 41 (1978).
[2] M. M. Thackeray, Prog. Solid State Chem. **25**, 1 (1997).
[3] J. M. Tarascon and M. Armand, Nature (London) **414**, 359 (2001).
[4] M. S. Whittingham, Chem. Rev. (Washington, D.C.) **104**, 4271 (2004).
[5] C. Delmas, C. Fouassier, and P. Hagenmuller, Physica B & C **99**, 81 (1980).
[6] P. Oliva, J. Leonardi, J. F. Laurent, C. Delmas, J. J. Braconnier, M. Figlarz, F. Fievet, and A. Deguibert, J. Power Sources **8**, 229 (1982).
[7] A. Van der Ven, D. Morgan, S. Y. Meng, and G. Ceder, J. Electrochem. Soc. **153**, A210 (2006).
[8] K. Koumoto, I. Terasaki, and R. Funahashi, MRS Bull. **31**, 206 (2006).
[9] K. Takada, Nature (London) **422**, 53 (2003).
[10] P. R. Somani and S. Radhakrishnan, Mater. Chem. Phys. **77**, 117 (2003).
[11] A. Van der Ven, G. Ceder, M. Asta, and P. D. Tepesch, Phys. Rev. B **64**, 184307 (2001).
[12] G. G. Amatucci, J. M. Tarascon, and L. C. Klein, J. Electrochem. Soc. **143**, 1114 (1996).
[13] A. Van der Ven, M. K. Aydinol, G. Ceder, G. Kresse, and J. Hafner, Phys. Rev. B **58**, 2975 (1998).
[14] A. Van der Ven, M. K. Aydinol, and G. Ceder, J. Electrochem. Soc. **145**, 2149 (1998).
[15] Z. H. Chen, Z. H. Lu, and J. R. Dahn, J. Electrochem. Soc. **149**, A1604 (2002).
[16] M. K. Aydinol, A. F. Kohan, G. Ceder, K. Cho, and J. Joannopoulos, Phys. Rev. B **56**, 1354 (1997).
[17] L. Benco, J. L. Barras, M. Atanosov, C. Daul, and E. Deiss, J. Solid State Chem. **145**, 503 (1999).
[18] R. Gomer, Rep. Prog. Phys. **53**, 917 (1990).
[19] S. R. de Groot and P. Mazur, *NonEquilibrium Thermodynamics* (Dover, Mineola, 1984).
[20] R. Zwanzig, J. Chem. Phys. **40**, 2527 (1964).
[21] G. Mazenko, J. R. Banavar, and R. Gomer, Surf. Sci. **107**, 459 (1981).
[22] B. J. Berne and R. Pecora, *Dynamic Light Scattering* (Dover, Mineola, 2000).
[23] A. B. Bortz, M. H. Kalos, and J. L. Lebowitz, J. Comput. Phys. **17**, 10 (1975).
[24] F. M. Bulnes, V. D. Pereyra, and J. L. Riccardo, Phys. Rev. E **58**, 86 (1998).
[25] G. H. Vineyard, J. Phys. Chem. Solids **3**, 121 (1957).
[26] J. M. Sanchez, F. Ducastelle, and D. Gratias, Physica A **128**, 334 (1984).
[27] D. De Fontaine, in *Solid State Physics*, edited by H. Ehrenreich and D. Trunbull (Academic, New York, 1994), p. 33.
[28] A. Van der Ven and G. Ceder, Phys. Rev. Lett. **94**, 045901 (2005).
[29] F. Zhou, G. Grigoryan, S. R. Lustig, A. E. Keating, G. Ceder, and D. Morgan, Phys. Rev. Lett. **95**, 148103 (2005).
[30] D. Morgan, J. D. Althoff, and D. de Fontaine, J. Phase Equilib. **19**, 559 (1998).
[31] A. Van der Ven and G. Ceder, Phys. Rev. B **71**, 054102 (2005).
[32] P. E. Blochl, Phys. Rev. B **50**, 17953 (1994).
[33] G. Kresse and D. Joubert, Phys. Rev. B **59**, 1758 (1999).

[34] G. Kresse and J. Furthmuller, Phys. Rev. B **54**, 11169 (1996).
[35] G. Kresse and J. Furthmuller, Comput. Mater. Sci. **6**, 15 (1996).
[36] J. R. Dahn and R. R. Haering, Solid State Commun. **40**, 245 (1981).
[37] K. Kang and G. Ceder, Phys. Rev. B **74**, 094105 (2006).
[38] S. A. Safran, Solid State Phys. **40**, 183 (1987).
[39] A. van de Walle and G. Ceder, J. Phase Equilib. **23**, 348 (2002).
[40] G. L. W. Hart, V. Blum, M. J. Walorski, and A. Zunger, Nat. Mater. **4**, 391 (2005).
[41] A. Van der Ven and G. Ceder, Electrochem. Solid-State Lett. **3**, 301 (2000).
[42] M. Catti, Phys. Rev. B **61**, 1795 (2000).
[43] M. Wilkening and P. Heitjans, Phys. Rev. B **77**, 024311 (2008).
[44] M. Wilkening, W. Kuchler, and P. Heitjans, Phys. Rev. Lett. **97**, 065901 (2006).
[45] B. G. Silbernagel and M. S. Whittingham, J. Chem. Phys. **64**, 3670 (1976).
[46] A. Honders, J. M. der Kinderen, A. H. van Heeren, J. H. W. de Wit, and G. H. J. Broers, Solid State Ionics **15**, 265 (1985).
[47] T. Yamamoto, S. Kikkawa, and M. Koizumi, Solid State Ionics **17**, 63 (1985).
[48] K. Matsumoto, R. Nagai, T. Asai, and S. Kawai, Solid State Ionics **25**, 233 (1987).
[49] K. Kanehori, F. Kirino, T. Kudo, and K. Miyauchi, J. Electrochem. Soc. **138**, 2216 (1991).
[50] W. Kuchler, P. Heitjans, A. Payer, and R. Schollhorn, Solid State Ionics **70-71**, 434 (1994).